



Dynamic response of buildings under debris flow impact

Huan LIU, Xiaoyi FAN, Shujun TIAN, Xin DENG

View online: <https://doi.org/10.1007/s11629-023-8572-x>

Articles you may be interested in

[Modeling of breaching parameters for debris flow dams](#)

Journal of Mountain Science. 2023, 20(10): 2835 <https://doi.org/10.1007/s11629-023-8052-3>

[Field observation of debris-flow activities in the initiation area of the Jiangjia Gully, Yunnan Province, China](#)

Journal of Mountain Science. 2022, 19(6): 1602 <https://doi.org/10.1007/s11629-021-7292-3>

[Dynamic response analysis of blocks-combined dam under impact load](#)

Journal of Mountain Science. 2020, 17(11): 2827 <https://doi.org/10.1007/s11629-019-5619-0>

[Debris flow impact on flexible barrier: effects of debris-barrier stiffness and flow aspect ratio](#)


Journal of Mountain Science. 2019, 16(7): 1629 <https://doi.org/10.1007/s11629-018-5314-6>



[The effects of rainfall regimes and rainfall characteristics on peak discharge in a small debris flow-prone catchment](#)


Journal of Mountain Science. 2019, 16(7): 1646 <https://doi.org/10.1007/s11629-018-5260-3>


Original Article

Dynamic response of buildings under debris flow impact

LIU Huan^{1,2,3}  <https://orcid.org/0009-0004-0673-3659>; e-mail: 202113000012@stu.swpu.edu.cn

FAN Xiaoyi^{2,4*}  <https://orcid.org/0000-0001-9001-1819>;  e-mail: fxy@swpu.edu.cn

TIAN Shujun⁵  <https://orcid.org/0000-0003-2058-6419>; e-mail: tsj19800702@163.com

DENG Xin²  <https://orcid.org/0009-0000-4911-6109>; e-mail: 979050531@qq.com

*Corresponding author

1 School of Mechanical and Electrical Engineering, Southwest Petroleum University, Chengdu 610500, China

2 School of Civil Engineering and Geomatics, Southwest Petroleum University, Chengdu 610500, China

3 Housing and Urban-Rural Development Bureau of Mingshan District, Ya'an 625100, China

4 Engineering Safety Assessment and Protection Research, Southwest Petroleum University, Chengdu 610500, China

5 School of Civil Engineering and Architecture, Southwest University of Science and Technology, Mianyang 621010, China

Citation: Liu H, Fan XY, Tian SJ, et al. (2024) Dynamic response of buildings under debris flow impact. Journal of Mountain Science 21(5). <https://doi.org/10.1007/s11629-023-8572-x>

© Science Press, Institute of Mountain Hazards and Environment, CAS and Springer-Verlag GmbH Germany, part of Springer Nature 2024

Abstract: This study employs the smoothed particle hydrodynamics–finite element method (SPH–FEM) coupling numerical method to investigate the impact of debris flow on reinforced concrete (RC)-frame buildings. The methodology considers the variables of debris flow depth and velocity and introduces the intensity index I_{DV} ($I_{DV} = DV$) to evaluate three different levels of debris flow impact intensity. The primary focus of this study is to investigate the dynamic response and failure mechanism of RC-frame buildings under debris flow impact, including structural failure patterns, impact force and column displacement. The results show that under a high-intensity impact, a gradual collapse process of the RC-frame building can be observed, and the damage mode of the frame column reflects shear failure or plastic hinge failure mechanism. First, the longitudinal infill walls are damaged owing to their low out-of-plane flexural capacity; the critical failure intensity index I_{DV} value is approximately 7.5 m²/s. The structure cannot withstand debris flows with an intensity index I_{DV} greater than 16 m²/s, and it is recommended that the peak impact force should not exceed 2100 kN. The

impact damage ability of debris flow on buildings mostly originates from the impact force of the frontal debris flow, with the impact force of the debris flow body being approximately 42% lower than that of the debris flow head. Finally, a five-level classification system for evaluating the damage status of buildings is proposed based on the numerical simulation and investigation results of the disaster site.

Keywords: SPH–FEM method; Debris flow; Buildings; The intensity index; Dynamic response

1 Introduction

Debris flow is a common natural disaster triggered by earthquakes, heavy rainfall, snowmelt and other factors. It is a solid–liquid two-phase fluid layer between sediment-laden water flow and block movement, such as landslides and rockfalls (Kattel et al. 2018), and is characterised by sudden eruption, high speed, large volume and strong destructive power (Sha et al. 2023). In recent decades, numerous studies have focused on large-scale landslides and debris flow

Received: 21-Dec-2023

Revised: 04-Feb-2024

Accepted: 12-Mar-2024

movements worldwide, along with their substantial impacts on buildings and infrastructures (Chen et al. 2012; Chen et al. 2016; Chen et al. 2020; Ciurean et al. 2017; Cui et al. 2022; Lei et al. 2022; Lin et al. 2018; Zhou et al. 2015). Therefore, studying the interaction between debris flow and structures is a challenging but crucial task (Chen et al. 2019). Furthermore, understanding the damage process and failure mechanism (Senthil et al. 2023) of buildings under the influence of debris flow movement is also important in assessing the vulnerability of buildings (Del Zoppo et al. 2022).

The current research methods in the field of debris flow-structure interaction can be classified into the following three categories. First is field investigation and statistical analysis (Chen et al. 2021; Hu et al. 2012b; Jakob et al. 2012; Kang and Kim 2016), which usually relies on specific data of disaster events, focusing on overall characteristics such as the runout distance, flow velocity, flow range and structural damage degree, without considering the clear interaction process between debris flow intensity and building damage. However, on-site investigation and statistical-analysis results can provide important references for experimental and numerical analysis models. The second is experimental research, in which researchers have already conducted flume model tests to study the impact mechanism and damage effects of debris flow movement on obstacles (Cui et al. 2015; Li et al. 2020; Li et al. 2021; Song et al. 2017; Vagnon and Segalini 2016; Wang et al. 2020; Zhou et al. 2018). However, due to the problems of scaling and simplifying model geometry structure, the test results are difficult to apply directly in engineering practices. The third is a numerical simulation, where researchers have explored the potential of using numerical tools to study the flow-structure interaction of rock and soil debris flows in recent years (Cheng et al. 2015; Gao et al. 2017; Li et al. 2018; Luo et al. 2020a; Luo et al. 2019a; Luo et al. 2020b; Zhang et al. 2018). The development of numerical simulation has deepened our understanding of the flow-structure interactions, including the influence of flow on structure (such as changing flow direction and range) and the influence of structure on flow. However, in calculating long-distance movement and large deformation of debris flow, the above finite element (FEM) mesh-based method may lead to serious mesh distortion. The calculation model has problems with load-structure coupling contact, such as not considering the load-structure coupling contact.

The smooth particle hydrodynamic method (SPH) is a meshfree approach (Feng et al. 2023) that exhibits strong adaptive characteristics. It can deal with large deformation problems and avoid calculation failure due to mesh distortion. It can also accurately simulate the mechanical properties of fluids. However, SPH has inherent defects, such as difficulty applying boundary conditions and low computational efficiency. Coupling SPH and FEM can take advantage of SPH in calculating large deformations and FEM in terms of accuracy and efficiency. Luo et al. (2022) utilised SPH–FEM coupling models to investigate the dynamic interaction between debris flows and rigid barriers, the energy dissipation of pebbles and the buffering mechanism of debris flows. Meanwhile, Feng et al. (2019) used the SPH–FEM coupling model to explore the dynamic impact problem of buildings affected by flow-like landslides in Shenzhen in 2015, and successfully reversed the entire process of building damage caused by landslides. These studies demonstrate the effectiveness and accuracy of the SPH–FEM coupling method in simulating rock and soil impact structures.

Therefore, previous studies explored the formation process and dynamic characteristics of debris flows, focusing on the influence of flow velocity and depth on their motion distribution and impact characteristics. However, the lack of literature on the coupling dynamic behaviour between debris flow and building structures limits the applicability of existing research results in practical engineering. To address this issue, the present study investigates the impact characteristics and failure mechanisms of building structures caused by debris flow velocity and flow depth. Using the SPH–FEM coupling numerical method, the study analyses the interaction between debris flow and buildings and the progressive collapse mechanism of typical RC-frame buildings. The method and results of this study can provide a certain reference for mountain building planning and design, as well as disaster prevention and reduction.

2 Interaction between Debris Flow and Buildings

2.1 Characteristics of the interaction

According to extensive field investigations and research on typical debris flow disasters, the dynamic interaction between debris flow and RC-frame

buildings mainly manifests in two forms. The first is sedimentation. It mainly occurs when debris flow passes through the building at a low velocity or enters the building, siltation accumulates around the building or inside the building (Fig. 1(a), (b)), but it will not cause major damage to the structural components (columns and beams), and the main damage mode is non-structural damage only to the wall. The second is the impact effect. It mainly acts on the frontal surface of the building, and individual structural members (usually columns and beams) can suffer serious damage or failure, but the entire structure will not collapse. But with the formation of plastic hinges for a few columns (Fig. 1(c)) or serious damage and even the collapse of the whole structure may occur, with the formation of plastic hinges at the top and bottom of most columns (Fig. 1(d), (e) and (f)). The main damage mode is structural damage owing to the failure of single structural elements (generally columns and beams) and even the collapse of the whole structure.

The interaction between debris flow and building is essentially the conversion between the kinetic energy of debris flow and the deformation internal energy of building. The destruction of building by debris flow is a process of material and energy transfer. Frontal impact is the main form of building structure damage, so this paper focuses on the dynamic response of RC-frame buildings under debris flow impact.

2.2 Damage mechanism of RC-frame buildings

Beams and columns are the main load-bearing

structures of RC-frame buildings, and the failure of columns usually leads to the loss of support and structural damage. The study found that when the failure ratio of the columns and beams exceeds 40%, the overall instability of the structure will be caused (Zeng et al. 2014a). Columns of RC structures are usually fixed on the beams, the ground floor and foundations. Their failure condition can be described by the formation of plastic hinges at the ends or in the midspan (Oguzhan and Shamim 2001). Based on the damage characteristics of RC-frame buildings in Qipangou debris flow, Zeng Chao (Zeng et al. 2014b) proposed two plastic hinge collapse at the ends of the RC column, three plastic hinge collapse at the ends and in the midspan of the column, and shear failure modes of the column.

Under lower debris flow impact intensity, the column generates elastic deformation. When the bending moment of debris flow applied on the column reaches the column's yield moment (M_c), the column begins to show plastic deformation, and a plastic zone appears at the fixed end of the column. When the external moment increases to the ultimate moment of the column (M_u), the plastic zone continues to deform and develops into plastic hinges at both ends. If the column is a non-load-bearing element, the plastic hinges at the ends will continue to transfer the external bending moment until the formation of plastic hinges at both ends and in the midspan of the column. Similarly, when the shear force produced by debris flow exceeds the ultimate shear force of the column, shear failure occurs.



Fig. 1 Building damage scenes in some typical debris flow-affected area. (a) (d) (e) Zhouqu debris flow; (b) (c) Longchi debris flow in Dujiangyan; (f) Qipangou debris flow in Wenchuan. (a) is from www.news.cn; (b) (c) were taken by the authors; (d) is from business.sohu.com; (e) is from blog.sina.com.cn; (f) is from Zeng et al. 2014b).

3 Method

3.1 Governing equations in SPH

The SPH is a Lagrangian and meshfree particle method that simulates fluid flow by discretising the computational domain into a series of interacting particles. It is used in this study to simulate the debris flow. The construction of SPH equations involves two key steps: kernel approximation and particle approximation (Feng et al. 2019). The Kernel approximation is applied to approximate the field variables' function through an integral representation by a smoothing kernel function W . In this way, the field variables can be introduced in a continuous form:

$$\langle f(r) \rangle = \int f(r') W(r-r', h) dr' \quad (1)$$

where $\langle \rangle$ represents the kernel approximation operator; $W(r-r', h)$ is the Kernel function whose value depends on the distance between two points $|r-r'|$ and the kernel radius κh ; h is the smooth length.

The smoothing kernel function W is an essential factor in SPH simulation. In this study, smoothing of the kernel function is the widely used cubic B-spline function with second-order accuracy (Feng et al. 2019).

Particle approximation is a process that the continuous form of the SPH kernel approximation is discretized into a summation of the influential surrounding particles. The process is conducted by estimating the field variables on these arbitrarily distributed particles within the support domain. Therefore, the final form of Eq. (1) is approximated as:

$$\begin{aligned} \langle f(r) \rangle &= \int f(r') W(r-r', h) dr' \\ &\approx \sum_{j=1}^N f(r_j) W(r-r_j, h) \Delta V_j \\ &= \sum_{j=1}^N f(r_j) W(r-r_j, h) \frac{1}{\rho_j} (\rho_j \Delta V_j) \\ &= \sum_{j=1}^N f(r_j) W(r-r_j, h) \frac{m_j}{\rho_j} \end{aligned} \quad (2)$$

where m_j , V_j and ρ_j represent the mass, volume, and density of particle j , respectively; N is the total number of particles within the support domain.

The value of the field function at particle i is obtained using the weighted average of the function values of all particles in the compact branch of the particle by the kernel function, as follows:

$$\begin{aligned} \langle f(r_i) \rangle &= \sum_{j=1}^N \frac{m_j}{\rho_j} f(r_j) W(r_i-r_j, h) \\ &= \sum_{j=1}^N \frac{m_j}{\rho_j} f(r_j) W_{ij} \end{aligned} \quad (3)$$

Similarly, the particle approximation for the space derivative of the field function at particle i becomes:

$$\langle \nabla \cdot f(r_i) \rangle = \sum_{j=1}^N \frac{m_j}{\rho_j} f(r_j) \cdot \nabla_i W_{ij} \quad (4)$$

Based on the above principle, the mass conservation equation and momentum conservation equation (Chen et al. 2019) can be expressed as:

$$\frac{d\rho_i}{dt} = \sum_{j=1}^N m_j v_{ij} \cdot \nabla_i W_{ij} \quad (5)$$

$$\frac{dv_i}{dt} = \sum_{j=1}^N m_j \left(\frac{\sigma_i^{\alpha\beta}}{\rho_i^2} + \frac{\sigma_j^{\alpha\beta}}{\rho_j^2} \right) \nabla_i W_{ij} + \frac{F_i}{m_i} \quad (6)$$

where v_{ij} is the relative velocity vector of particles i and j ; $\sigma_i^{\alpha\beta}$ and $\sigma_j^{\alpha\beta}$ are the total stress tensors composed of isotropic pressure and deviational stress; superscripts α and β represent coordinate directions; F_i is a variety of external forces, such as gravity, friction, contact force, etc.

3.2 SPH–FEM coupling algorithm

To simulate the interaction between debris flow and RC-frame buildings, the SPH-FEM coupling algorithm is used for simulation. The debris flow is simulated by SPH and the buildings are simulated by FEM. A node-to-surface contact algorithm is adopted to transfer displacements and contact forces between the debris flow and the buildings, with SPH particles acting as the contact slave node and FEM elements acting as the main contact plane. The contact theory adopts the penalty function algorithm (Chen et al. 2019) to apply the force from the node to the finite element. The basic principle of the penalty function involves adding a contact spring and damping between the SPH particle and the FEM element to limit particle penetration through the main plane. Fig. 2 depicts the contact model used in this study.

It is recommended to check if the SPH particles penetrate the main face at each time step. When a penetration occurs, a contact force exists between the SPH particles and the main surface. Normal contact force f_n and tangential contact force f_t (Liu et al. 2021) are as follows:

$$f_n = -k_n \delta_n + c_n \dot{\delta}_n \tag{7}$$

$$f_t = \begin{cases} -k_t \delta_t + c_t \dot{\delta}_t, & f_n \mu > -k_t \delta_t + c_t \dot{\delta}_t \\ f_n \mu, & f_n \mu \leq -k_t \delta_t + c_t \dot{\delta}_t \end{cases} \tag{8}$$

where k_n and k_t are normal and tangential spring stiffness, respectively; δ_n and δ_t are normal and tangential penetration displacements, respectively; c_n and c_t are normal and tangential damping coefficients, respectively; μ is the friction coefficient.

k_n and k_t are calculated in a similar way and have the same size.

$$k_n = k_t = \begin{cases} k_1 \frac{KA}{L}, & \text{for shell} \\ k_1 \frac{KA^2}{V}, & \text{for solid} \end{cases} \tag{9}$$

where k_1 is the scale factor of interface stiffness, which is usually defaulted to 0.1; K is the bulk modulus of the material; A is the area of the contact section element; L is the maximum diagonal length of the shell element; V is the contact unit volume.

3.3 Model validation

To evaluate the performance of the present method in describing flow-structure interaction, a granular flow model test conducted by Moriguchi (Moriguchi et al. 2009) is simulated. The schematic diagram of the geometric model is shown in Fig. 3(a). The flume is designed with a length of 1.8 m and a width of 0.3 m, and the inclination angle of the flume is adjustable (45°, 55°, and 65°). A sand box of 0.045 m³ (0.3 m × 0.3 m × 0.5 m).

The coupled SPH-FEM numerical analysis method is used to reproduce the whole test process. The numerical simulation parameters are consistent with the debris flow impact test and the finite element simulation parameters conducted by Moriguchi (Moriguchi et al. 2009) and Lee (Lee et al. 2019). The debris flow in the test is simulated by SPH particles, and the flume and load cell are simulated by FEM. The mesh and meshless model of numerical simulation are shown in Fig. 3(b).

Fig. 4 shows the comparison of the impact process for the debris flow impact test and the numerical

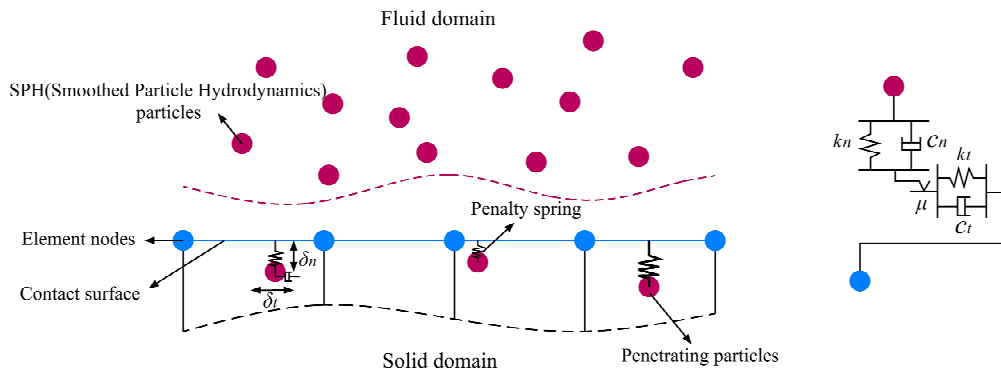


Fig. 2 Contact model between fluid particles and solid elements.

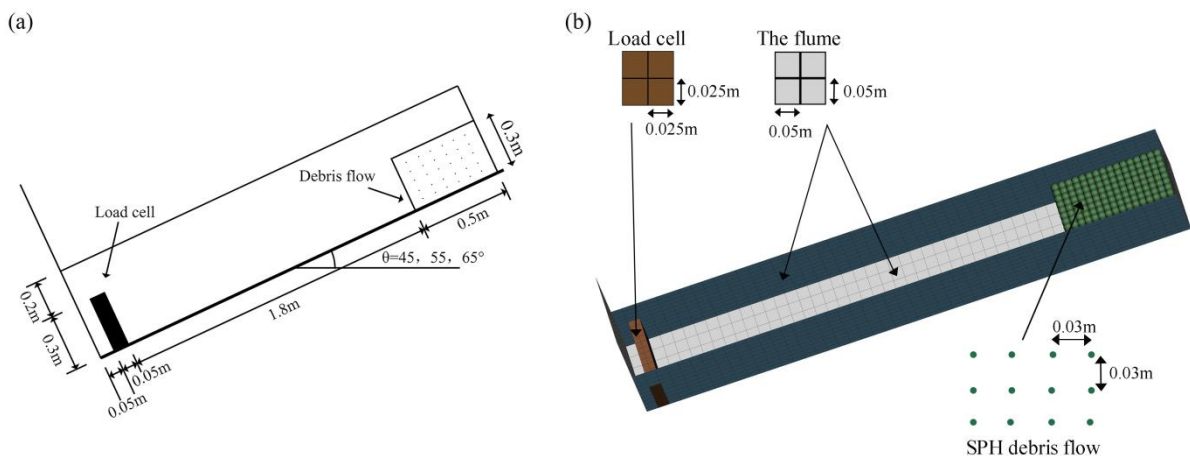


Fig. 3 Schematic diagram of the flume model: (a) geometric mode; (b) mesh and meshless model.

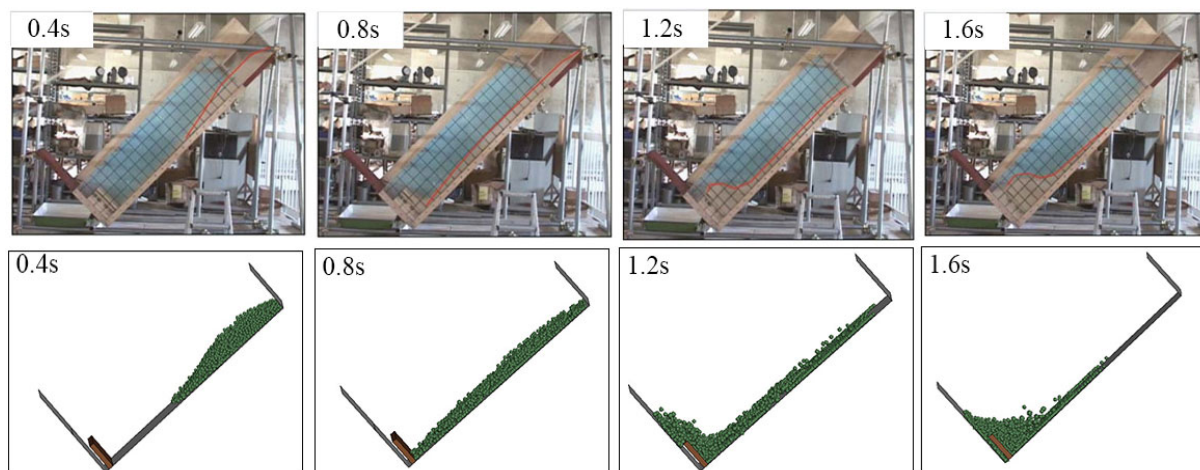


Fig. 4 Comparison of the impact process for the debris flow impact test and the numerical simulation.

simulation at different times ($t = 0.4s, t = 0.8s, t = 1.2s, t = 1.6s$), with a flume slope of 45° . In this analysis, gravity is defined as the only loading condition. The debris flow is suddenly released at $t = 0s$. When $t = 0.8s$, it reaches the bottom of the flume, hitting the rigid wall. The experimental results are consistent with the numerical simulation of the flow process.

In the numerical analysis, the total impact force is the value of the contact force between debris flow and load cell. The total impact force is calculated as the sum of the normal forces on the load cell ($0.3m \times 0.3m$). Fig. 5 compares the experimental and numerical results with the time-varying impact force. The comparison reveals that both the peak and residual impact forces are well captured by the present method. The error rate is $2.0\% \sim 9.7\%$, which meets the requirements of assessment. Meanwhile, in the existing research results (Liu et al. 2024), the effectiveness of the reinforced concrete structure model is verified by comparing and analyzing the

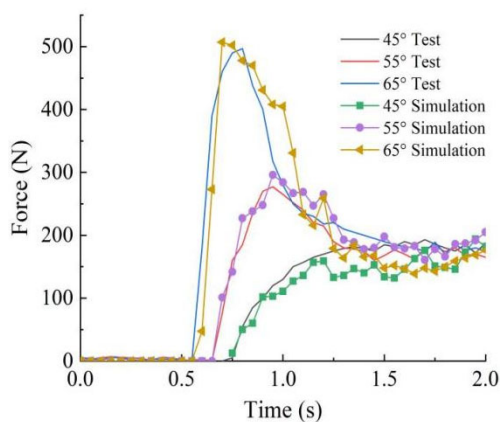


Fig. 5 Comparison between laboratory experiments and simulated impact force.

damage characteristics of simulated and actual debris flow damaged building structures. The above results illustrate the applicability and reliability of the SPH-FEM coupled numerical model to simulate the flow-structure interaction. In the following section, the method will be used to simulate the dynamic interaction between debris flow and buildings.

4 Model Setup

4.1 Numerical model

Through the field investigation and measurement of the debris flow in Qipangou, Zeng Chao obtained 98 building damage samples (Zeng et al. 2014a). Among them, the long axis direction of a two-story frame structure is perpendicular to the flow direction of debris flow. The debris flow damages the infill walls and columns, ultimately causing the building to lose stability and collapse. This paper takes it as an example and establishes the overall model, as shown in Fig. 6(a). The global model is created using 3D (three-dimensional) modelling software consisting of a RC-frame building, debris flow slurry, rigid ground and a baffle. The volume of the debris flow is $20m \times 20m \times 2m / 3m / 4m / 5m / 6m$. The size of the rigid ground is $50m \times 21m \times 0.02m$, whereas the rigid baffle on both sides measures $50m \times 7m \times 0.02m$. Initially, the distance between the front end of the debris flow and the building is $3m$.

The building model adopts a two-story reinforced concrete frame structure with a total length of $10.8m$, a width of $5.4m$ and a height of $6m$ in accordance with the conventional design standards of buildings in rural

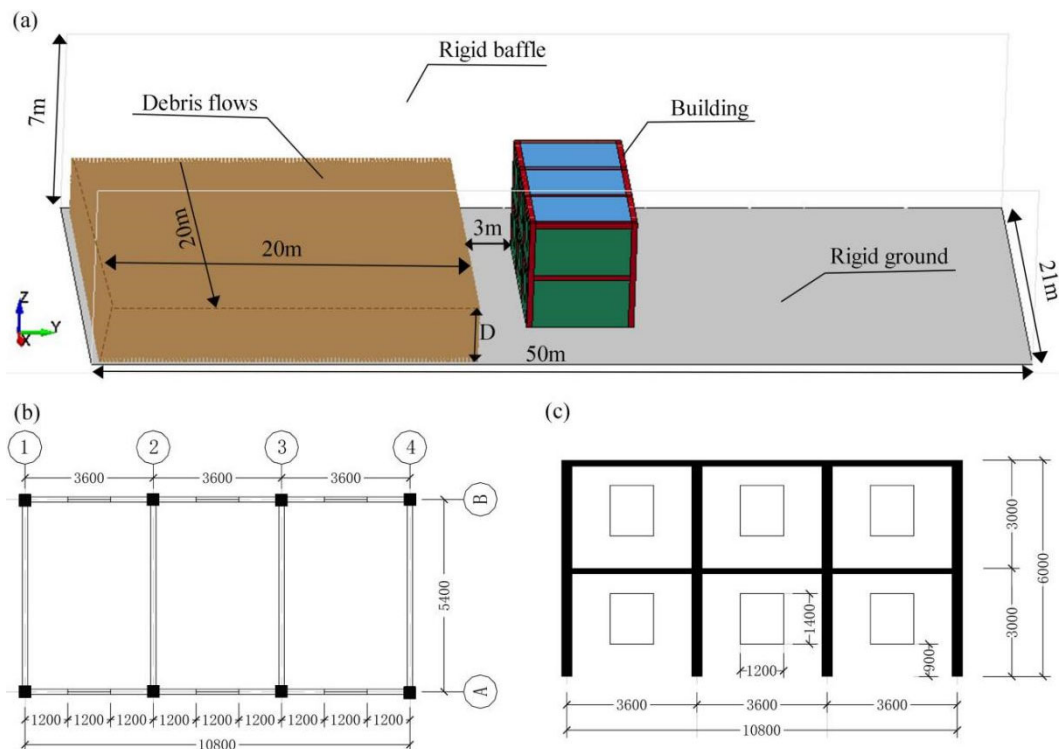


Fig. 6 Numerical model: (a) global model; (b) top view of building model (unit: mm); (c) front view of building model (unit: mm).

areas of China. The frame columns and beams have cross-sectional dimensions of 300 mm × 300 mm, with the infill walls and floor slabs having a thickness of 150 mm. The steel reinforcements of the frame columns and beams consist of 8Φ14 longitudinal steel reinforcements and Φ8@200 stirrups, whereas the floor slab has transverse and longitudinal steel reinforcements of Φ14@200. The window size is 1.2 m × 1.4 m and is located 0.9 m from the bottom of the wall. Since doors and windows are assumed to have no resistance to the impact of debris flow, they are not included in the model. Figs. 6(b) and (c) depict the specific geometric dimensions of the building model.

4.2 Material model

Concrete material: The frame column, beam and slab members are made of C25 concrete. The concrete material adopts the continuous cap model (MAT_CSCM_CONCRETE), and its failure criterion adopts the maximum principal strain. When the maximum principal strain of the component of concrete material exceeds 0.05, the concrete element fails.

Masonry filling wall material: The HJC damaged material model (MAT_JOHNSON_HOLMQUIST_CONCRETE) is

used to simulate the masonry filling wall, and the failure criterion of the maximum principal strain was adopted. The masonry filling wall element fails when the maximum principal strain exceeds 0.0033.

Steel reinforcement material: The ideal elastic-plastic material model (MAT_PLASTIC_KINEMATIC) is adopted. The material properties are as follows: a material density of 7850 kg/m³, elastic modulus of 200 GPa and Poisson's ratio of 0.3. The failure of the principal strain is set to 0.1. The longitudinal and transverse steel reinforcements of the structural members have a yield strength of 400 MPa, whereas the stirrups have a yield strength of 300 MPa.

Material of debris flow slurry: Debris flow slurry is a complex non-Newtonian fluid, primarily consisting of gravel, sand and water. Due to its intricate constitutive relationship and dynamic properties, it is often approximated using the elastic-plastic fluid dynamics material model (MAT_ELASTIC_PLASTIC_HYDRO) and an equation of state (EOS). EOS is used to update the pressure term, defined as a linear polynomial equation of state with weak compressibility. When the coefficient C_1 of the first polynomial equation is used alone, the elastic modulus cannot be used for deformation beyond the elastic range. The smooth

SPH particles are used to simulate debris flow slurry, and the spacing of SPH particles is 0.2 m.

Rigid material: The ground and baffle are modelled using the MAT_RIGID material model, which enhances the speed and efficiency of the analysis but also prevents structural penetration during the simulation. The rigid material has a density of 3000 kg/m³, an elastic modulus of 30 GPa and a Poisson ratio of 0.24. The above material parameters are summarised in Table 1.

The erosion technology algorithm is often used to ensure numerical convergence in the simulation (Luo et al. 2019b), removing any element from the calculation that reaches a specified failure threshold and is assumed to have no resistance to any loading. In this study, the failure criteria for concrete (beams, slabs, columns), masonry (filled walls) and steel reinforcements are based on the maximum principal strain of the model material. When the maximum principal strain of a material is reached, the programme automatically deletes the corresponding element. By utilising the erosion algorithm, the progressive collapse process of the building can be observed.

4.3 Calculation elements

The simulation for columns, beams, slabs and infill walls employs solid elements, with a total of 70362 solid elements. The reinforcement is simulated using beam elements, comprising 14564 beam elements. Furthermore, the ground and baffle are simulated using shell elements, with 8200 shell elements. The debris flow is simulated using SPH particles, with the number of particles varying with the depth of the debris flow. For instance, at a flow depth of 3 m, there are 163216 particles. HyperMesh software is used to divide the model. In order to save calculation time and ensure calculation accuracy, the minimum mesh element size of each component is kept as close as possible.

4.4 Contact interfaces, boundary conditions and loadings

In order to establish contact between the debris flow slurry and the frame column, beam, plate, filling wall, ground and baffle, automatic point-surface

Table 1 Material parameters of model.

Material	Parameters	Value	Reference
Concrete (MAT_CSCM_CONCRETE)	Density, ρ (kg·m ⁻³)	2400	Liu et al. 2019
	Unconfined compressive strength, (MPa)	25	
	Maximum aggregate size, (mm)	20	
	Erosion coefficient	1.1	
	Recovery coefficient	10	
Masonry infill wall (MAT_JOHNSON_HOLMQUIST_CONCRETE)	Failure strain	0.05	Xu et al. 2012
	Density, ρ (kg·m ⁻³)	2000	
	Shear modulus, G (MPa)	1000	
	Quasi-static uniaxial compressive strength, (MPa)	3.33	
Steel reinforcement (MAT_PLASTIC_KINEMATIC)	Crushing pressure, (MPa)	16	Luo et al. 2019b
	Failure strain	0.0033	
	Density, ρ (kg·m ⁻³)	7850	
	Young's modulus, E (GPa)	200	
	Poisson's ratio, ν	0.3	
Debris flow slurry (MAT_ELASTIC_PLASTIC_HYDRO+LINEAR POLYNOMIAL EOS)	Yield stress, (MPa)	400/300	Liu et al. 2021
	Failure strain	0.1	
	Density, ρ (kg·m ⁻³)	2000	
	Shear modulus, G (MPa)	1.7	
	Plastic hardening modulus, (KPa)	3	
Rigid materials (MAT_RIGID)	Yield stress, (KPa)	5	Liu et al. 2021
	Polynomial equation coefficient, C_0 - C_6 (GPa)	$C_1 = 5,$ $C_0, C_2-C_6 = 0$	
	Density, ρ (kg·m ⁻³)	3000	
	Young's modulus, E (GPa)	30	
	Poisson's ratio, ν	0.24	

contact (Contact_Automatic_Nodes_to_Surface) is used. The static and dynamic friction coefficients are set at 0.2 and 0.12 (Liu et al. 2019), respectively.

The numerical model used in this study does not consider the foundation of the building. The bottom of the building is subjected to fixed boundary conditions for the ground. A common node connects the columns, beam and slabs of the building. In practice, for simulating the connection effect of tensile steel reinforcements, the connection between the frame column and the infill wall is achieved by consolidating adjacent grid elements with a spacing of 0.5 m along its height direction. The steel reinforcement element is embedded in the concrete element, and CONSTRAINED_LAGRANGE_IN_SOLID defines the constraint between the steel reinforcement and the concrete (Luo et al. 2019b). This method ensures the conservation of momentum and balance of force, as the force deformation of the steel reinforcement and concrete is the same.

The numerical model considers the self-weight of the building, and the gravitational acceleration is set to 9.8 m/s². Following the Load Code for the Design of Building Structures (Luo et al. 2019b), a uniformly distributed load of 2.0 kN/m² is applied to the top surface of the slab and roof without considering other loads, such as wind and seismic loads. In this study, it is assumed that the debris flow direction is perpendicular to the long-axis direction of the RC-frame building, and the debris flow impacts the front side of the building. The total simulation time is set to 3.0 s for simulating the entire process of the debris flow impacting the building.

4.5 Working condition parameters

The main variable parameters in this article are

flow velocity and depth. Considering the debris flow accumulation area with buildings distributed, the flow velocity of debris flow can generally reach 4m/s (Lei et al. 2016), and the flow velocity of debris flow causing the complete destruction of RC-frame buildings needs to be about 9.4m/s (Kang and Kim 2016). Especially the most severe debris flow disaster since the founding of the People's Republic of China, namely the " 8.8 " catastrophic debris flow disaster in Zhouqu, Gansu, China. According to on-site investigation and remote sensing image analysis (Hu et al. 2012a), after the Sanyanyu debris flows out of the mountain pass, it forms a deposition area in the urban area, with a sedimentation thickness of about 2 m to 7 m and an average thickness of about 4 m. The maximum flow velocities at the outlet of Sanyanyu and Luojiayu are 9.9 m/s and 5.5 m/s, respectively. Meanwhile, in combination with this study, a two-story RC-frame building is adopted, with a total height of 6 m. Therefore, in the numerical simulation, four flow velocities of 4 m/s, 6 m/s, 8 m/s and 10 m/s are set respectively, and five flow depths of 2 m, 3 m, 4 m, 5 m and 6 m are set correspondingly. The impact damage degree of the debris flow on the buildings is evaluated using the intensity index I_{DV} ($I_{DV}=DV$), which is divided into three grades of low, moderate and (relatively) high based on the research method of literature (Jakob et al. 2012; Luo et al. 2019b). Table 2 depicts the specific working condition parameters.

5 Result Analysis and Discussion

5.1 Impact process

Fig. 7 presents the simulation process to illustrate the impact of debris flow on a building with a flow depth of 3 m (equivalent to the height of the first floor

Table 2 Working condition parameters and building damage mode

Condition number	D (m)	V (m/s)	I_{DV} (m ² /s)	Impact intensity level	Upstream walls	Downstream walls	Structural components	Overall building
D2V6	2	6	12	Low	Damaged	Undamaged	No failure	No collapse
D3V4	3	4	12	Low	Damaged	Undamaged	No failure	No collapse
D2V8	2	8	16	Moderate	Damaged	Damaged	Partial failure	No collapse
D4V4	4	4	16	Moderate	Damaged	Damaged	No failure	No collapse
D3V6	3	6	18	(relatively) High	Damaged	Damaged	Failure	Gradual collapse
D2V10	2	10	20	High	Damaged	Damaged	Failure	Collapse
D3V8	3	8	24	High	Damaged	Damaged	Failure	Collapse
D4V6	4	6	24	High	Damaged	Damaged	Failure	Collapse
D5V4	5	4	20	High	Damaged	Damaged	Failure	Collapse
D6V4	6	4	24	High	Damaged	Damaged	Failure	Collapse

Note: D, Flow depth; V, Flow velocity; I_{DV} , Intensity index.

of the building) and a flow velocity of 6 m/s (designated as working condition D3V6). At $t = 0$, the debris flow starts to move at an initial velocity of 6 m/s and accelerates due to gravity. As shown in Figs. 7(a) and (e), at $t = 0.45$ s, the frontal debris flow reaches the building and causes the upstream walls of the building to fail, leading to partial concrete damage of two frame columns. As the debris flow material flows into the building, the two damaged frame columns in the front row are further compromised, which results in the tearing and damaging of the filling wall of the second-floor frame, as shown in Fig. 7(f). At $t = 1.25$ s, the debris flow reaches the back-filling wall of the building and causes it to fail, as demonstrated in Fig. 7(b). During this process, the building structure blocks some of the debris flow, leading to part of the debris flow slurry running up along the wall and column, whereas the rest of the debris flow slurry spreads to both sides around the building and flows downward. As shown in

Fig. 7(c), at $t = 2.0$ s, the two frame columns in the back row are damaged, and the filling wall of the second floor in the back row is cracked and damaged. In the last 3.0 s, the continuous impact of debris flow causes the front and back frame columns to intensify damage, ultimately making the building unstable, as shown in Fig. 7(g). Due to friction, the debris flow eventually stops flowing and accumulates around the building, as shown in Fig. 7(d). The simulation accurately depicts the process of debris flow starting movement, impact climbing, flow diffusion, stable sedimentation, etc.

5.2 Building damage pattern under disaster intensity

The damage characteristics of the upstream walls, downstream walls, structural components (columns) and the overall building are revealed by impact tests conducted at three different intensity levels, i.e. low,

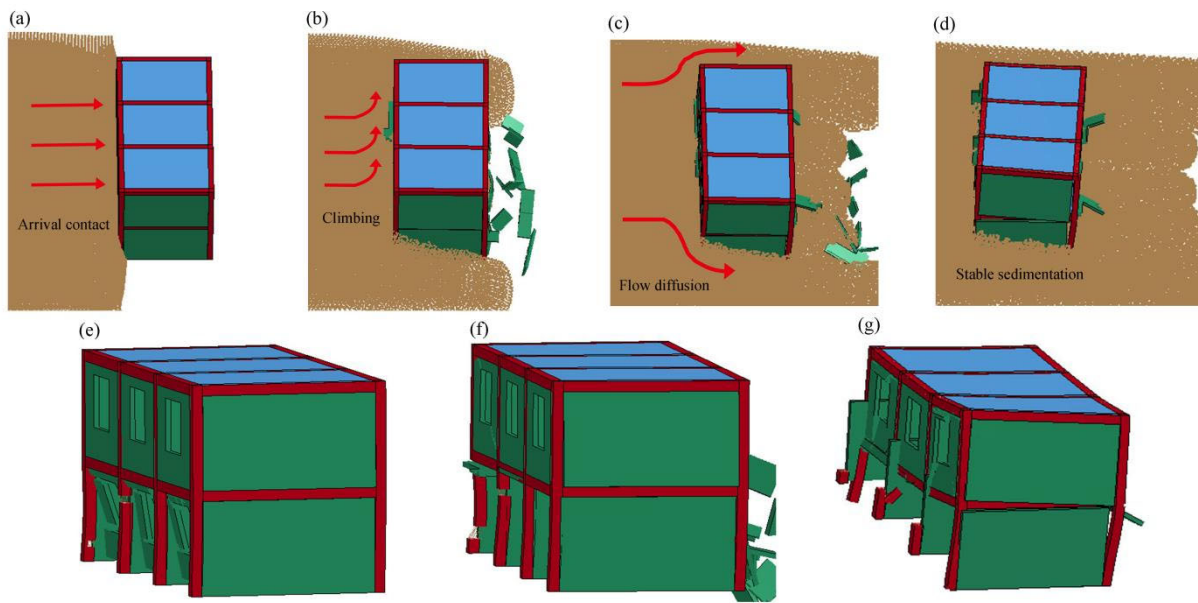


Fig. 7 Process of debris flow impacting the building ($D = 3$ m, $V = 6$ m/s). Impact process: (a) $t = 0.45$ s, (b) $t = 1.25$ s, (c) $t = 2.0$ s, (d) $t = 3.0$ s; Building damage pattern: (e) $t = 0.45$ s, (f) $t = 1.25$ s, (g) $t = 3.0$ s.

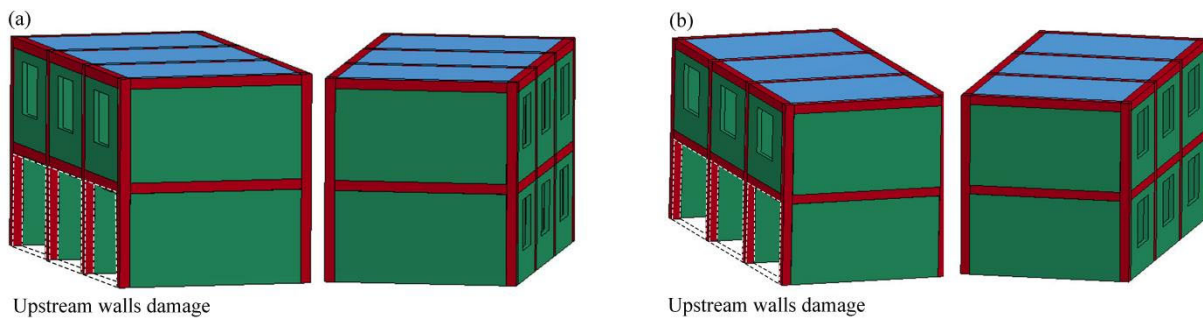


Fig. 8 Damage patterns of buildings under low impact intensity: (a) $D = 2$ m, $V = 6$ m/s; (b) $D = 3$ m, $V = 4$ m/s.

moderate and relatively high. A damage matrix model of walls damage, components failure (including shear failure, plastic hinge, etc.), and overall collapse for the RC-frame building is established, as shown in Table 2. When the depth and velocity of the debris flow are $D \geq 2$ m and $V \geq 6$ m/s, or $D \geq 3$ m and $V \geq 4$ m/s, respectively, the upstream walls are damaged. When $D \geq 2$ m and $V \geq 8$ m/s, or $D \geq 3$ m and $V \geq 6$ m/s, or $D \geq 4$ m and $V \geq 4$ m/s, the downstream walls are damaged. The structural components fail when $D \geq 2$ m and $V \geq 10$ m/s or $D \geq 3$ m and $V \geq 6$ m/s. When $D \geq 2$ m and $V \geq 10$ m/s, or $D \geq 3$ m and $V \geq 8$ m/s, or $D \geq 4$ m and $V \geq 6$ m/s, or $D \geq 5$ m and $V \geq 4$ m/s, the overall collapse of the building occurs.

Fig. 8 depicts the damage pattern of the building at low impact intensity. The upstream walls are damaged, mainly due to the low out-of-plane flexural capacity. The debris flow enters the interior of the building and reaches the downstream walls. At this point, the I_{DV} value of the debris flow intensity index is about $7.5 \text{ m}^2/\text{s}$. Due to the low kinetic energy of the debris flow, the downstream walls and main load-bearing components remain undamaged. Similar building damage patterns are observed in Fig. 1(b) at the Longchi debris flow disaster site in Dujiangyan, Sichuan Province. The building is shielded by other buildings at the impact front of the debris flow and is located at the far end of the flow. When the debris flow arrives, the kinetic energy of the impact is small, causing only damage to the walls, and the building remains stable as a whole.

Fig. 9 presents the damage pattern of the building under moderate impact intensity. After the upstream walls fail, debris flow enters the building and damages the downstream walls. Simultaneously, the impact of the debris flow affects the front two frame columns. The concrete in the lower part falls off in a large area, and the stressed steel reinforcement yields, resulting in partial damage and destruction of the middle columns. However, under this intensity of impact, the kinetic energy of the debris flow is not enough to cause damage to the other main load-bearing components of the frame, and the overall structure remains stable. Similar building damage patterns are observed in Fig. 1(c) at the Longchi debris flow disaster site in Dujiangyan, Sichuan Province.

Fig. 10 depicts the instability pattern of the building under high impact intensity. Unlike the moderate impact condition, due to the high-intensity impact of the debris flow, the frame columns and walls suffer serious damage, and the entire frame becomes unstable and collapses. The main body of the building is washed away by the debris flow, resulting in complete destruction. The failure of the frame columns is mainly due to the debris flow reaching its ultimate bending moment or ultimate shear force, which reflects the failure mechanism of a plastic hinge or shear failure mechanism. Fig. 1(f) presents the damage to the building at the Qipangou debris flow in Wenchuan, Sichuan (Zeng et al. 2014b). The columns

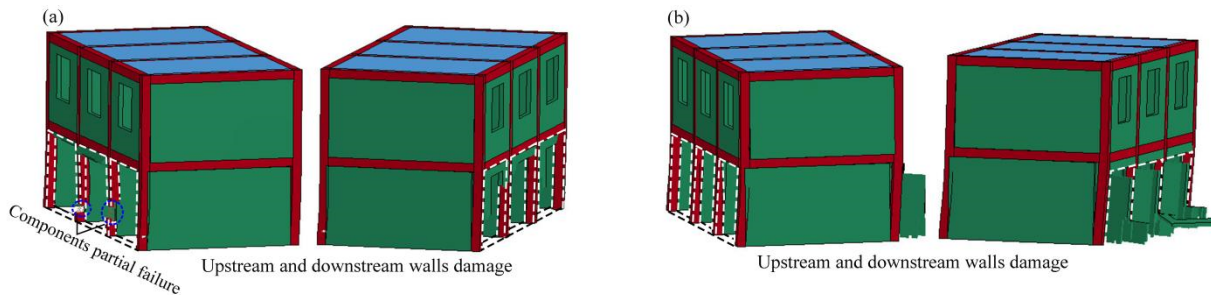


Fig. 9 Damage patterns of buildings under moderate impact intensity: (a) $D = 2$ m, $V = 8$ m/s; (b) $D = 4$ m, $V = 4$ m/s.

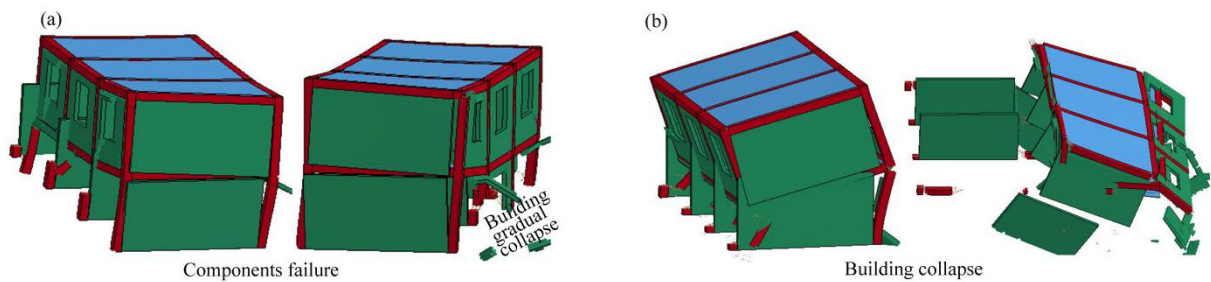


Fig. 10 Damage patterns of buildings under high impact intensity: (a) $D = 3$ m, $V = 6$ m/s. (b) $D = 2$ m, $V = 10$ m/s; $D = 3$ m, $V = 8$ m/s; $D = 4$ m, $V = 6$ m/s; $D = 5$ m, $V = 4$ m/s; $D = 6$ m, $V = 4$ m/s.

and beams of the building are either directly cut or a plastic hinge is produced by the debris flow, and eventually the entire frame structure falls in the direction of the debris flow movement.

5.3 Impact force

Fig. 11 illustrates the time history curve of a RC-frame building subjected to the impact force of debris flow. The peak value of the impact force increases with the increase in flow depth and the velocity of debris flow. At low impact intensity (D2V6, D3V4) and moderate impact intensity (D2V8, D4V4), the overall stability of the building structure is maintained. The impact force curve exhibits two peaks corresponding to the front and rear frames of the debris flow impact on the building, namely the two rows of frame columns and walls jointly subjected to the impact force of the debris flow. The debris flow vertically impacts the front facade of the building, initially acting on the frame columns, beams, and infill walls in the front row. The impact force on the building decreases sharply with the damage to the infill walls and some frame columns in the front row. At this stage, the impact force is primarily supported by the frame columns. Subsequently, the peak impact force of the frame columns and filled walls in the rear row decreased by an average of about 42% due to the resistance of the structure and the frictional energy consumption of the debris flow. However, under high impact intensity, the building loses stability and collapses, and the impact force curve shows a peak value followed by a rapid decrease.

Under low impact intensity, the upstream wall of the building incurs damage, and the corresponding peak impact forces are 1350 kN and 1399 kN for working conditions D2V6 and D3V4, respectively. Under moderate impact intensity, both the upstream and downstream walls of the building suffer impact damage. The peak impact forces for working conditions D2V8 and D4V4 are 2101 kN and 2134 kN, respectively. Under relatively high impact intensity (working condition D3V6), the building undergoes a gradual process of instability characterised by "walls damage - components failure - overall collapse," and the peak impact force is 2193 kN. Under high impact intensity, the building rapidly collapses, and the corresponding peak impact force exceeds 2300 kN.

The RC-frame building designed according to the standard in this article cannot withstand debris flows with an intensity index I_{DV} ($I_{DV}=DV$) greater than 16

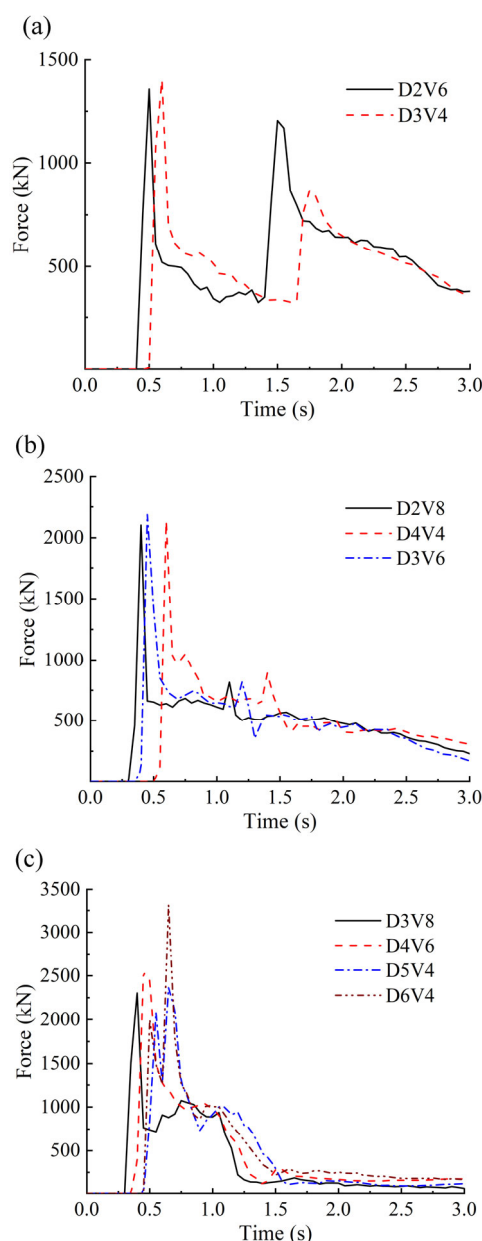


Fig. 11 Time-history curves of impact force: (a) low-impact intensity case; (b) moderate-impact and relatively high-impact intensity case; (c) high-impact intensity case.

m²/s. It is recommended that the peak value of the corresponding ultimate impact force does not exceed 2100 kN. To withstand larger-scale debris flows, further research is required on protecting RC-frame buildings under the action of debris flows. The primary protective measures include strengthening the buildings and setting up retaining structures.

5.4 Column displacement

Fig. 12(a) depicts the distribution position of the

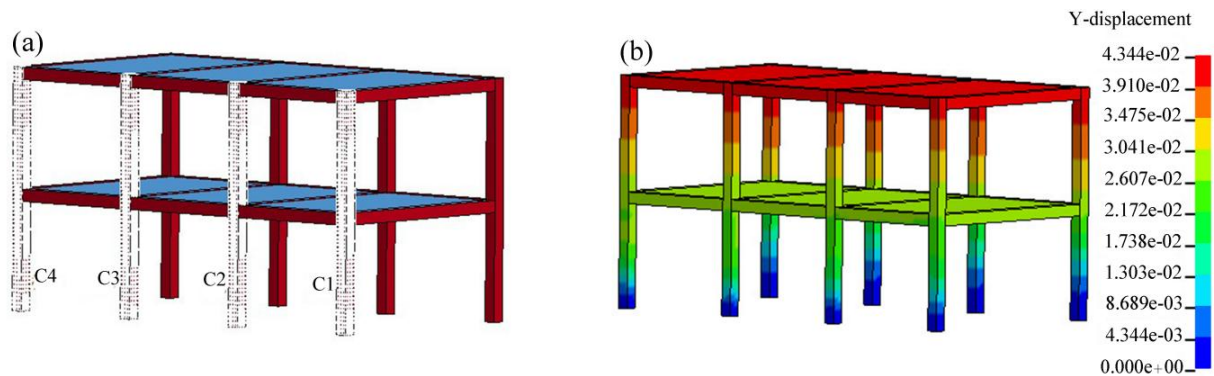


Fig. 12 (a) Distribution position of front row columns; (b) Y-direction displacement contours of columns (unit: m).

front-row columns. Fig. 12(b) presents that the maximum displacement of the frame columns during the debris flow impact is concentrated at the top position by analysing the Y-direction displacement contours of the frame columns under the impact of debris flow with a depth of 3 m and velocity of 4 m/s (working condition D3V4). The displacement change process is further studied by plotting the displacement time-history curves to obtain a more comprehensive understanding of the displacement of the front-row columns.

In Fig. 13, C1 (D3V4) represents the front frame column 1 under the impact of debris flow depth of 3 m and velocity of 4 m/s. The displacement curve numbers are the same below. The displacement of the frame column increases with the debris flow depth and velocity increase. The overall change trend of the frame column curve is consistent, as shown in Figs. 13 (a), (b) and (c), with working condition D3V4 used as an example. Under the impact of debris flow with a depth of 3 m and velocity of 4 m/s, the displacement and deformation curves of the frame column almost overlap in the first 1 s, and the maximum displacement is about 0.04 m. After 1 s, due to the combined effect of the resistance of the building structure and the impact of debris flow, the upper displacement of the column slightly decreases, resulting in small deformation and reciprocating waves. Corner column 4 has a displacement of about 0.01 m, higher than other frame columns, but this can be ignored compared to the total height of frame columns of 6 m. For the frame building that maintains overall stability under the impact of debris flow, the displacement curve shows that the deformation of the frame column is completed in a very short time, from the beginning of deformation to the maximum about 0.25 s. It can be concluded that the impact damage ability of debris flow mainly comes from the frontal debris flow. Therefore, if the structure

can withstand the impact of the frontal debris flow, it can avoid the risk of collapse of the overall structure.

In Fig. 13 (d), under the impact of debris flow with a depth of 3 m and velocity of 6 m/s, the debris flow begins to act on the building at 0.5 s. The front corner of column 4 is partially damaged, and the displacement on the column rapidly increased to 0.12 m. At 1.25 s, the debris flow washes out the rear wall and part of the rear corner column, which is aggravated by the rapid increase of the load on the front column. The displacement on the columns increased rapidly, and the maximum displacement of column 4 reached 0.77 m. Figs. 13 (e) and (f) show that the front frame column is damaged when debris flows in these five working conditions come into contact and collide with buildings. Due to the large impact energy of debris flow, the displacement on the column increases almost linearly.

5.5 Evaluation of damage grade of RC-frame buildings

With the rapid development of the national mountain economy and the improvement of people's living standards, especially with the overall promotion of the rural revitalisation policy after the country has achieved overall prosperity, the structural form of new buildings in mountain areas has evolved from masonry to brick concrete and frame structures in recent years (Lei et al. 2016). In the future, frame structures will be the main type of buildings in mountainous areas prone to debris flow geological disasters. Luo et al. (2023) summarised the vulnerability of buildings to landslide and debris flow disasters in recent years. The building structures under the impact of a single landslide or debris flow hazard are the most concerned in the literature, which is also the focus of the current research.

In evaluating the extent of damage and failure of

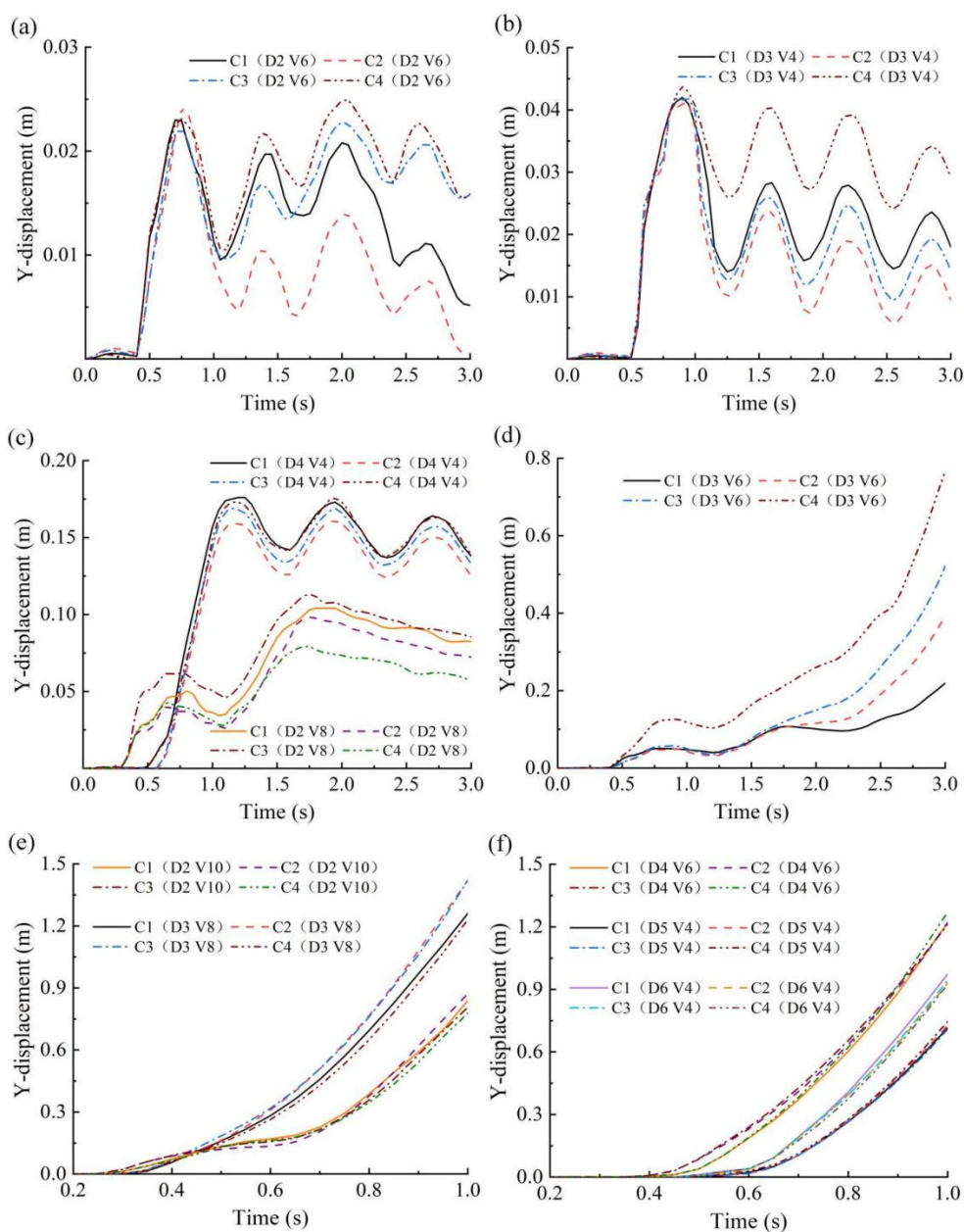


Fig. 13 Displacement curves of front frame column. (a) low-impact intensity case (D2V6); (b) low-impact intensity case (D3V4); (c) moderate-impact intensity case (D4V4 and D2V8); (d) relatively high-impact intensity case (D3V6). (e) high-impact intensity case (D2V10 and D3V8); (f) high-impact intensity case (D4V6, D5V4 and D6V4).

the RC-frame building, it is essential to determine its failure state and the intensity of the debris flow. This report utilises a combination of numerical simulation, existing disaster field investigation results and relevant research findings (Hu et al. 2012b; Luo et al. 2019b). Thus, a semi-quantitative classification standard is presented, which offers a clear and objective framework for assessing the level of damage inflicted on RC-frame buildings by debris flow. The standard comprises five levels of damage, namely very slight damage, slight damage, moderate damage, severe

damage and complete damage (Table 3). The intensity index I_{DV} interval in the Table 3 is the recommended value range based on the classification of debris flow affected by intensity grade during the numerical simulation. The degree of damage to buildings ranges from 0 (no damage) to 1 (complete damage), with values based on existing literature (Kang and Kim 2016; Luo et al. 2019b).

The intensity of debris flow can be expressed by flow depth D , velocity V , impact pressure P , dynamic impact force DV^2 and overturning moment DV in

Table 3 Evaluation of damage grade of RC-frame buildings.

Damage class	Damage description	Damage scale	Case scenario	Intensity index I_{DV} (m^2/s)
Complete	Most load-bearing structural components (columns and beams) are severely damaged, leading to the collapse of the entire building or the translation of the remaining building, or the burial thickness is more than 2 stories	Subject structural damage or loss of functionality	Fig. 10 high impact intensity cases; Fig. 1 (e) (f) shows complete collapse	>18
Severe	Severe damage or collapse of multiple load-bearing structural components, resulting in partial collapse of the building, or the burial thickness is greater than 1 story but less than 2 stories	Partial structural damage or partial loss of functionality	Fig. 1 (d) case in Zhouqu debris flow	(16, 18]
Moderate	Non-load-bearing walls are seriously damaged, individual load-bearing structural components are damaged, but the building as a whole does not collapse, or the burial thickness is less than 1 story	Individual structural damage or reduced functionality	Fig. 9 moderate impact intensity cases; Fig. 1 (c) Longchi debris flow in Dujiangyan	(12, 16]
Slight	Cracks on non-load bearing walls or severe damage to external walls; there is no obvious damage to the load-bearing structural components, or the buried thickness is less than 0.5 story	No structural damage, some non-structural function damage	Fig. 8 low impact intensity cases; Fig. 1 (b) Longchi debris flow in Dujiangyan	(7.5, 12]
Very slight	Only non-structural components (windows and doors) are damaged slightly; the main load-bearing structural components (columns and beams) and secondary structural components (slabs and infill walls) are intact, or sediment accumulation on the ground	Minor damage to non-structural parts, easy to repair	Fig. 1 (a) the building in Zhouqu debris flow	≤ 7.5

literature (Zhang et al. 2018). Among them, dynamic impact force DV^2 and overturning moment DV are more suitable, and DV is also a common index for flood risk assessment. Although the appropriate strength index DV is used, there are still some limitations in this manuscript. Firstly, due to the limited number of numerical simulation samples and the limited number of reference strength indicators for RC-frame structure failure under debris flow at home and abroad. In addition, different building codes in different countries may lead to significant differences in strength index values. Therefore, the intensity index of debris flow in Table 3 is within the recommended range of values. Meanwhile, the damaged building in this study is a two-story RC-frame building. The degree of damage depends not only on the type of structure, but also on the shape, orientation, location, etc., which requires a more detailed classification of the damaged buildings. Therefore, it is necessary to further study the damaged RC-frame buildings.

6 Conclusions

In this study, the dynamic response of typical buildings under the impact of debris flow is

investigated by constructing a numerical model for the coupling between RC-frame buildings and debris flow using the SPH-FEM method. The conclusions are listed as follows:

(1) The SPH-FEM coupled numerical method can effectively simulate the processes of climbing, flow diffusion, and stable sedimentation when debris flow impacts the RC-frame building. The simulated damage pattern of the building structure is similar to the actual damage characteristics in the debris flow disaster site, thus confirming the accuracy of the coupled numerical method and model.

(2) The study found that low-intensity debris flow causes damage only to the front row infill walls of a building. Moderate-intensity debris flow damages the front and rear rows of infill walls, but the overall stability of the building remains intact. However, high-intensity debris flow causes severe damage to the front and rear frame columns and walls, leading to the collapse of the entire frame and the destruction of a building.

(3) The longitudinal filled wall is the first to be damaged due to its low out-of-plane bending ability, and its critical failure strength index I_{DV} is about 7.5 m^2/s . Frame columns are crucial load-bearing components of building structures, and their failure

leads to a progressive building collapse. The structure cannot withstand debris flow with an intensity index greater than 16 m²/s.

(4) The displacement curves of the frame column indicate that the maximum deformation occurs within 0.25 s of the impact of the debris flow, after which it fluctuates within a small range. This suggests that the impact of debris flow damage is primarily caused by the force of the frontal debris flow, with the impact force of the debris flow body decreasing by about 42% relative to the head. Therefore, if the structure can withstand the impact of the frontal debris flow, it can avoid the risk of a complete structural collapse.

(5) Based on the results of numerical simulations and field investigations of previous disasters, a five-level classification system has been proposed to evaluate the damage state of buildings. This system effectively reflects the progressive development of building damage and comprehensively discusses the progressive destruction process of typical RC-frame buildings. The classification of damage degree and the physical description of the damage state provides a reliable basis for accurate building damage evaluation, thereby promoting scientific research on building vulnerability assessment. The vulnerability of the buildings to debris flow can be assessed quantitatively based on the identified failure process, failure mechanisms and impact intensity index, which can

promote the development of a quantitative risk assessment of debris flow.

Acknowledgments

This work was supported by the National Natural Science Foundation of China (Grant No. 41877524, No. 42172320, No. 41971214).

Author Contribution

LIU Huan: Investigation, Methodology, Software, Writing – original draft, Writing – review & editing. FAN Xiao-yi: Conceptualization, Funding acquisition, Validation, Project administration, Supervision. TIAN Shu-jun: Resources, Supervision. DENG Xin: Data curation, Software, Visualization.

Ethics Declaration

Availability of Data: Data will be available from the corresponding author upon reasonable request.

Conflict of Interest: The authors declare no conflict of interest.

References

- Chen HX, Li J, Feng SJ, et al. (2019) Simulation of interactions between debris flow and check dams on three-dimensional terrain. *Eng Geol* 251: 48-62.
<https://doi.org/10.1016/j.enggeo.2019.02.001>
- Chen HX, Zhang LM, Chang DS, et al. (2012) Mechanisms and runoff characteristics of the rainfall-triggered debris flow in Xiaojiagou in Sichuan Province, China. *Nat Hazards* 62(3): 1037-1057.
<https://doi.org/10.1007/s11069-012-0133-5>
- Chen HX, Zhang LM, Gao L, et al. (2016) Simulation of interactions among multiple debris flows. *Landslides* 14(2): 595-615.
<https://doi.org/10.1007/s10346-016-0710-x>
- Chen M, Tang C, Zhang X, et al. (2021) Quantitative assessment of physical fragility of buildings to the debris flow on 20 August 2019 in the Cutou gully, Wenchuan, southwestern China. *Eng Geol* 293: 106319.
<https://doi.org/10.1016/j.enggeo.2021.106319>
- Chen Q, Chen L, Gui L, et al. (2020) Assessment of the physical vulnerability of buildings affected by slow-moving landslides. *Nat Hazards Earth Syst Sci* 20(9): 2547-2565.
<https://doi.org/10.5194/nhess-20-2547-2020>
- Cheng XS, Zhang AJ, Ren Y (2015) Failure mechanism and anti-collapse measures of masonry structure under debris flow. *Engineering Mechanics* 32(08): 156-163. (In Chinese).
<https://doi.org/doi:10.6052/j.issn.1000-4750.2014.01.0084>
- Ciurean RL, Hussin H, van Westen CJ, et al. (2017) Multi-scale debris flow vulnerability assessment and direct loss estimation of buildings in the Eastern Italian Alps. *Nat Hazards* 85(2): 929-957.
<https://doi.org/10.1007/s11069-016-2612-6>
- Cui P, Zeng C, Lei Y (2015) Experimental analysis on the impact force of viscous debris flow. *Earth Surf Processes Landforms* 40(12): 1644-1655.
<https://doi.org/10.1002/esp.3744>
- Cui Q, Zhang LL, Chen XY, et al. (2022) Quantitative risk assessment of landslides with direct simulation of pre-failure to post-failure behaviors. *Acta Geotechnica* 17(10): 4497-4514.
<https://doi.org/10.1007/s11440-022-01485-w>
- Del Zoppo M, Di Ludovico M, Protà A (2022) A mechanics-based method towards risk assessment of RC buildings under tsunami and flow-type hazards. *Eng Struct* 264.
<https://doi.org/10.1016/j.engstruct.2022.114452>
- Feng D, Yi C, Hu M, et al. (2023) Simulation of non-cohesive soil turning based on a SPH model. *Comput Geotech* 160.
<https://doi.org/10.1016/j.compgeo.2023.105502>
- Feng SJ, Gao HY, Gao L, et al. (2019) Numerical modeling of interactions between a flow slide and buildings considering the destruction process. *Landslides* 16(10): 1903-1919.
<https://doi.org/10.1007/s10346-019-01220-9>
- Gao L, Zhang LM, Chen HX (2017) Two-dimensional simulation of debris flow impact pressures on buildings. *Eng Geol* 226: 236-244.
<https://doi.org/10.1016/j.enggeo.2017.06.012>

- Hu KH, Cui P, Ge YG (2012a) Building destruction patterns by August 8, 2010 debris flow. *J Mountain Sci* 30(4): 484-490. (In Chinese).
<https://doi.org/10.16089/j.cnki.1008-2786.2012.04.020>
- Hu KH, Cui P, Zhang JQ (2012b) Characteristics of damage to buildings by debris flows on 7 August 2010 in Zhouqu, Western China. *Nat Hazards Earth Syst Sci* 12(7): 2209-2217.
<https://doi.org/10.5194/nhess-12-2209-2012>
- Jakob M, Stein D, Ulmi M (2012) Vulnerability of buildings to debris flow impact. *Nat Hazards* 60(2): 241-261.
<https://doi.org/10.1007/s11069-011-0007-2>
- Kang HS, Kim YT (2016) The physical vulnerability of different types of building structure to debris flow events. *Nat Hazards* 80(3): 1475-1493.
<https://doi.org/10.1007/s11069-015-2032-z>
- Kattel P, Kafle J, Fischer JT, et al. (2018) Interaction of two-phase debris flow with obstacles. *Eng Geol* 242: 197-217.
<https://doi.org/10.1016/j.enggeo.2018.05.023>
- Lee K, Kim Y, Ko J, et al. (2019) A study on the debris flow-induced impact force on check dam with- and without-entrapment. *Comput Geotech* 113.
<https://doi.org/10.1016/j.compgeo.2019.103104>
- Lei Y, Cui P, Jiang X (2016) Failure mechanism and structure optimization of masonry building due to debris flow impact. *Journal of Sichuan University* 48(04): 61-69. (In Chinese).
<https://doi.org/10.15961/j.jsuese.2016.04.009>
- Lei Y, Gu HH, Cui P (2022) Vulnerability assessment for buildings exposed to torrential hazards at Sichuan-Tibet transportation corridor. *Eng Geol* 308: 106803.
<https://doi.org/10.1016/j.enggeo.2022.106803>
- Li P, Li T, Lu Z, et al. (2018) Parametric study on dynamic response of FRP masonry structures under the impacts of debris flow. *Shock Vib*. 2018: 1-20.
<https://doi.org/10.1155/2018/4527571>
- Li P, Rong K, Lu Z, et al. (2020) Experimental and numerical study on the performance of novel RC frame structure encased with shaped steel under debris flow impact. *Eng. Struct.* 212: 110472.
<https://doi.org/10.1016/j.engstruct.2020.110472>
- Li P, Xu S, Lu Z, et al. (2021) Experimental study on the performance of CFRP-strengthened masonry structures under debris flow impacts. *Structures* 31: 602-612.
<https://doi.org/10.1016/j.istruc.2021.02.014>
- Lin F, Wu LZ, Huang RQ, et al. (2018) Formation and characteristics of the Xiaoba landslide in Fuquan, Guizhou, China. *Landslides* 15(4): 669-681.
<https://doi.org/10.1007/s10346-017-0897-5>
- Liu C, Yu Z, Luo L, et al. (2019) Dynamic behavior of a concrete dam impacted by debris flows with rock. *Journal of Vibration and Shock* 38(14): 161-168 (in Chinese).
<https://doi.org/doi:10.13465/j.cnki.jvs.2019.14.023>
- Liu C, Yu Z, Zhao S (2021) A coupled SPH-DEM-FEM model for fluid-particle-structure interaction and a case study of wenjia gully debris flow impact estimation. *Landslides* 18(7): 2403-2425.
<https://doi.org/10.1007/s10346-021-01640-6>
- Liu H, Fan XY, Jiang YJ, et al. (2024) Dynamic response of frame structure building under impact of debris flow with large stones. *Journal of Vibration and Shock* 43(1): 9-19 (in Chinese).
<https://doi.org/10.13465/j.cnki.jvs.2024.01.002>
- Luo G, Zhao Y, Shen W, et al. (2022) Dynamics of bouldery debris flow impacting onto rigid barrier by a coupled SPH-DEM-FEM method. *Comput. Geotech.* 150: 104936.
<https://doi.org/10.1016/j.compgeo.2022.104936>
- Luo HY, Fan RL, Wang HJ, et al. (2020a) Physics of building vulnerability to debris flows, floods and earth flows. *Eng Geol* 271: 105611.
<https://doi.org/10.1016/j.enggeo.2020.105611>
- Luo HY, Shen P, Zhang LM (2019a) How does a cluster of buildings affect landslide mobility: A case study of the Shenzhen landslide. *Landslides* 16(12): 2421-2431.
<https://doi.org/10.1007/s10346-019-01239-y>
- Luo HY, Zhang L, Zhang L, et al. (2023) Vulnerability of buildings to landslides: The state of the art and future needs. *Earth-Sci. Rev.* 238: 18.
<https://doi.org/10.1016/j.earscirev.2023.104329>
- Luo HY, Zhang LL, Zhang LM (2019b) Progressive failure of buildings under landslide impact. *Landslides* 16(7): 1327-1340.
<https://doi.org/10.1007/s10346-019-01164-0>
- Luo HY, Zhang LM, Wang HJ, et al. (2020b) Multi-hazard vulnerability of buildings to debris flows. *Eng Geol* 279: 105859.
<https://doi.org/10.1016/j.enggeo.2020.105859>
- Moriguchi S, Borja RI, Yashima A, et al. (2009) Estimating the impact force generated by granular flow on a rigid obstruction. *Acta Geotechnica* 4(1): 57-71.
<https://doi.org/10.1007/s11440-009-0084-5>
- Oguzhan B, Shamim S (2001) Plastic hinge analysis. *J. Struct. Eng.* 127(9): 1092-1100.
- Senthil K, Thakur A, Singh AP, et al. (2023) Transient dynamic response of brick masonry walls under low velocity repeated impact load. *Int. J. Impact Eng.* 174.
<https://doi.org/10.1016/j.ijimpeng.2023.104521>
- Sha S, Dyson AP, Kefayati G, et al. (2023) Simulation of debris flow-barrier interaction using the smoothed particle hydrodynamics and coupled eulerian lagrangian methods. *Finite Elem. Anal. Des.* 214.
<https://doi.org/10.1016/j.finel.2022.103864>
- Song D, Ng CWW, Choi CE, et al. (2017) Influence of debris flow solid fraction on rigid barrier impact. *Can Geotech J* 54(10): 1421-1434.
<https://doi.org/10.1139/cgj-2016-0502>
- Vagnon F, Segalini A (2016) Debris flow impact estimation on a rigid barrier. *Nat. Hazards Earth Syst. Sci.* 16(7): 1691-1697.
<https://doi.org/10.5194/nhess-16-1691-2016>
- Wang D, Li Q, Bi Y, et al. (2020) Effects of new baffles system under the impact of rock avalanches. *Eng Geol* 264.
<https://doi.org/10.1016/j.enggeo.2019.105261>
- Xu H, Yu Z, Kang X, et al. (2012) Numerical simulation on collapse process of multistory masonry structure in earthquake. *Building Structure* 42(S1): 220-225 (in Chinese).
[https://doi.org/doi:10.02-848X\(2012\)S1-0220-06](https://doi.org/doi:10.02-848X(2012)S1-0220-06)
- Zeng C, Cui P, Ge Y, et al. (2014a) Characteristics and mechanism of buildings damaged by debris flows on 11 July, 2013 in Qipangou of Wenchuan, Sichuan. *Journal of Earth Sciences and Environment* 36(2): 81-91.
[https://doi.org/1672-6561\(2014\)02-0081-11](https://doi.org/1672-6561(2014)02-0081-11)
- Zeng C, Cui P, Su Z, et al. (2014b) Failure modes of reinforced concrete columns of buildings under debris flow impact. *Landslides* 12(3): 561-571.
<https://doi.org/10.1007/s10346-014-0490-0>
- Zhang S, Zhang L, Li X, et al. (2018) Physical vulnerability models for assessing building damage by debris flows. *Eng Geol* 247: 145-158.
<https://doi.org/10.1016/j.enggeo.2018.10.017>
- Zhou GGD, Cui R, Tang JB, et al. (2015) Experimental study on the triggering mechanisms and kinematic properties of large debris flows in Wenjia Gully. *Eng Geol* 194: 52-61.
<https://doi.org/10.1016/j.enggeo.2014.10.021>
- Zhou GGD, Song D, Choi CE, et al. (2018) Surge impact behavior of granular flows: Effects of water content. *Landslides* 15(4): 695-709.